ChemComm

COMMUNICATION

View Article Online
View Journal | View Issue

Published on 11 November 2014. Downloaded by Michigan State University on 20/01/2016 17:53:46.

Cite this: *Chem. Commun.*, 2015, 51, 421

Received 5th September 2014,
Accepted 6th November 2014

DOI: 10.1039/c4cc06968d

www.rsc.org/chemcomm

Multicolor imaging and the anticancer effect of a bifunctional silica nanosystem based on the complex of graphene quantum dots and hypocrellin A†

Lin Zhou,[a] Lin Zhou,[b] Xuefeng Ge,[a] Jiahong Zhou,*[a] Shaohua Wei*[a] and Jian Shen[a]

An effective theranostic platform based on porous silica nanoparticles encapsulated with the complex of a photodynamic anticancer drug and graphene quantum dots (GQDs), with the bifunction of multicolor imaging and satisfactory photo-induced anticancer activity, was successfully designed and prepared for *in vitro* photodynamic therapy (PDT) of superficial cancer.

PDT was proposed as a useful tool in oncology.[1] The therapeutic effect of PDT is activated by photoexcitation of the localized photosensitizers (PSs) to generate cytotoxic reactive oxygen species, *e.g.*, singlet oxygen ($^1O_2$), free radicals, or peroxides, to selectively and irreversibly destroy diseased tissues.[2] The use of theranostic agents, combining therapy and imaging, which enable the online imaging of a drug for the detection of disease, image-guided drug delivery and treatments, guidance of surgical resection, and monitoring of treatment response, is an emerging interdiscipline that paves the way towards the goal of personalized PDT treatment.[3]

It is well known that the penetration depth of light is inversely proportional to the wavelength. So, from the light penetration depth point of view, conventional fluorescent materials, such as organic dyes and quantum dots, excited by visible light, were not ideal imaging probes because their activation light penetration depth was not deep enough to penetrate the solid tumor inside the body.[4] Furthermore, autofluorescence of the organism and the weak resistance to photobleaching of conventional fluorescent materials may also affect their detection effect and veracity.[5] However, the advantage of applying visible light triggering theranostic reagents for superficial cancer, such as skin, vessel or intraluminal cancer, which can be treated directly using optical fibers inside the body, is that they would cause less tissue heating and damage to the deep normal tissue.[6] Therefore, it is meaningful to develop effective visible light triggering theranostic reagents for PDT and imaging for superficial cancer.

Hypocrellin A (HA, Scheme S1, ESI†) is an efficient PS, especially suitable for superficial diseases because its spectral absorption almost coincides with the phototherapeutic window of superficial diseases (480–600 nm);[7] in addition, over the wavelength area of 480–600 nm, HA possess higher photodynamic activity than many widely used PSs.[6a,8] GQDs, a class of C-dots, have received increasing attention, owing to their outstanding fluorescence properties, low toxicity and good resistance to photo-degradation and bleaching, which showed great potential in the field of biological theranostics.[3a,9] Most importantly, GQDs can easily form complexes with aromatic drugs through π–π stacking interaction without complicated synthetic steps, which are not general and not always possible.

Here, the complex of HA and GQD (HA–GQD) was prepared through π–π stacking interaction to get multicolor imaging and PDT activity, simultaneously. Multicolor fluorescence imaging is superior to the single color one, especially in visible light triggering imaging, since repeatedly multicolor corroboration can avoid errors in judgment from autofluorescence of the organism. As shown in Scheme 1, to avoid the complex separation during the drug delivery process and

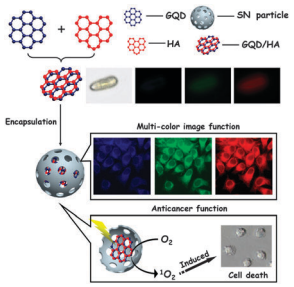

Scheme 1 Schematic representation of HA–GQD–SiO_2 and its bifunction of multicolor imaging and PDT of cancer cells.

[a] *College of Chemistry and Materials Science, Analysis and Testing Centre, Jiangsu Key Laboratory of Biofunctional Materials, Jiangsu Collaborative Innovation Centre of Biomedical Functional Materials, Key Laboratory of Applied Photochemistry, Nanjing Normal University, Wenyuan Road No. 1, Nanjing, China. E-mail: zhoujiahong@njnu.edu.cn, shwei@njnu.edu.cn; Fax: +86-25-85898170; Tel: +86-25-85898170*

[b] *School of Chemistry & Chemical Engineering, Jiangsu University, Xuefu Road No. 301, Zhenjiang, China. Fax: +86-511-88791800; Tel: +86-511-88791800*

† Electronic supplementary information (ESI) available: Experimental procedures, the molecular structure of HA, detailed information about UV-Vis, CD patterns, zeta potential, lifetime, and fluorescence microscopy. See DOI: 10.1039/c4cc06968d

Published on 11 November 2014. Downloaded by Michigan State University on 20/01/2016 17:53:46.

further improve the fluorescence signal intensity and PDT activity, HA–GQD was encapsulated inside porous silica nanoparticles (HA–GQD–SiO_2). On the one hand, porous SiO_2 does not release the entrapped HA–GQD to avoid complex separation; and on the other, the porous matrix of SiO_2 is permeable to light and molecular as well as oxygen and $^1O_2$ to make sure the imaging and PDT activity. Therefore, the desired imaging and PDT effect of HA–GQD will be maintained even in the encapsulated form.[2d] Furthermore, the silica shell protection could also avoid the negative effect for imaging and PDT efficacy from massive complicated substances in the body.

The synthesis of the HA–GQD complex was performed based on π–π stacking interaction. Encapsulation of HA–GQD inside porous silica nanoparticles was carried out by an improve sol–gel method in aqueous solution to avoid the separation of HA–GQD.[10] Full experimental details can be found in the ESI.†

To understand the interaction mechanisms between HA and GQDs and make sure formation of HA–GQD, their fluorescence properties were studied. After HA was added to GQD solution, the fluorescence intensity of GQDs reduced gradually (Fig. 1A), indicating the fluorescence quenching of GQD by HA. This fluorescence quenching possibly could be ascribed to the energy or electron transfer from GQDs to HA.[11] The Stern–Volmer curve, the peak intensity as a function of the concentrations of HA, was plotted and the curve showed upward exponential behavior, which can be attributed to combined dynamic and static quenching or solely static quenching largely. Dynamic quenching refers to a process where the GQD and HA come into contact during the lifetime of the excited state, whereas static quenching refers to GQD–HA complex formation. Such upward exponential behavior was usually interpreted in terms of a "sphere of action" and described using the modified S–V equation:[12]

$$F_0/F = (1 + K_D[Q])\exp([Q]V)$$

where F_0 and F represent the corrected GQD fluorescence intensities in the absence and presence of HA. $[Q]$ is the concentration of HA; and K_D and V are dynamic and static quenching constants, respectively.

To determine the fluorescence quenching mechanism of GQDs by HA, the nanosecond fluorescence lifetime of GQD was measured using the time correlation single photon counting (TCSPC) technique (details are in ESI†). As shown in Fig. 1B and Table S1 (ESI†), with the increase in HA concentration, the $\tau_{average}$ of systems sharply decreased from 1.571 to 0.201 ns. Furthermore, the proportion of each component was also greatly changed. These results reveal the strong interaction between GQDs and HA, which indicated that the contribution of dynamic quenching should be completely ruled out and the quenching process becomes purely static, which indicated the formation of the HA–GQD complex.[12] The static quenching constant was determined to be $V = 13.15 \times 10^{-3}$ $(\text{mg mL}^{-1})^{-1}$.

Time-resolved fluorescence spectroscopy (TRES), a useful analysis of intermolecular interaction dynamics, of HA–GQD showed that after being excited by 370 nm nano-LED, the GQD portion of HA–GQD was quickly excited and showed the fluorescence signal at about 450 nm (ESI,† Fig. S3). In contrast, the HA exciting signal (about 600 nm) was not detected until the exciting time was increased to 306.2–307.1 ns (1395–1399 channel, time calibration = 2.194787×10^{-10} s per channel). After that, with the increase in GQD fluorescence intensity, the fluorescence intensity of HA gradually increased, which indicated that there is energy transfer from GQD to HA. After the GQD fluorescence intensity reached a maximum at 316.0–316.9 ns (1440–1444 channels) and then dropped down, the fluorescence intensity of HA was only slightly increased and reached a maximum at 318.2–319.1 ns (1450–1454 channels). The fluorescence intensity of HA was increased when the GQD was fully excited, which demonstrated that there is energy transfer from GQDs to HA. However, such an increasing degree was not very big, which implied that the energy transfer from GQDs to HA is not the main reason for the fluorescence quenching of GQDs by HA. Furthermore, the energy transfer efficiency calculation results also show that there are both energy and electron transfer processes from GQDs to HA and the electron transfer mechanism is the main reason for such fluorescence quenching (ESI†). When the HA–GQD complex was formed, the superior fluorescence properties of GQDs can be maintained at our experiment interaction ratio.

GQD has small influence on the fluorescence properties of HA, which indicated that such interaction could not obviously affect the photo-excitation process of HA, and possibly do not affect its PDT effect (Fig. S4 and Table S2, ESI†).

To avoid the complex separation during drug delivery process and further improve the fluorescence signal intensity and PDT activity, HA–GQD was encapsulated inside porous silica nanoparticles. A TEM image of the HA–GQD–SiO_2 is shown in Fig. 2A. The particles are spherical, having uniform size distribution. In order to get more evidence to verify that HA–GQD has been successfully embedded into silica nanocarriers and determine the structure of silica nanoparticles, fluorescence quenching experiments were conducted using triethylamine (TA) and the iodide ion

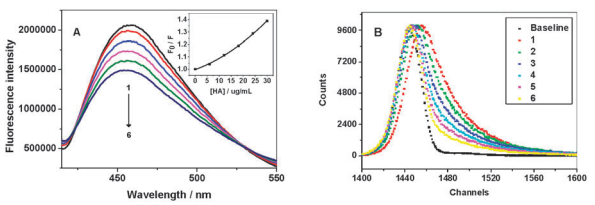

Fig. 1 (A) Fluorescence spectra of GQDs with the increase of HA (inset panel: Stern–Volmer plots for the quenching of GQD fluorescence by HA); (B) time-resolved fluorescence decays for GQDs in the absence and presence of HA (370 nm nano-LED as the exciter and the signal at 450 nm of GQD was detected). [GQD] = 150 μg mL^{-1}; [HA] 1–6 = 0, 6, 12, 18, 24, 30 μg mL^{-1}.

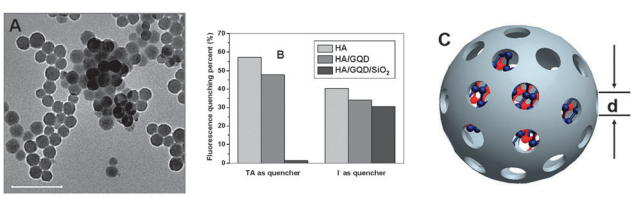

Fig. 2 (A) TEM image of HA–GQD–SiO_2 (scale bar = 200 nm); (B) fluorescence quenching efficacy of HA, HA–GQD and HA–GQD–SiO_2 by TA and I^-; (C) structure of HA–GQD embedded silica nanoparticles (0.440 nm < d < 0.624 nm).

 This journal is © The Royal Society of Chemistry 2015

Published on 11 November 2014. Downloaded by Michigan State University on 20/01/2016 17:53:46.

(I^-) as fluorescence quenchers for the HA portion of HA–GQD. The results in Fig. 2B indicated that when TA was used as a fluorescence quencher, the fluorescence of HA and HA–GQD was quenched remarkably, but no obvious quenching was detected for HA–GQD–SiO_2, which indicated that HA–GQD was successfully encapsulated inside silica nanoparticles and TA cannot diffuse into silica nanoparticle from the pore on the surface of silica nanoparticles. In contrast, I^- can efficiently quench the fluorescence HA, HA–GQD and HA–GQD–SiO_2, which demonstrated that I^- can diffuse into silica nanoparticles and subsequently quench the fluorescence of the embedded HA–GQD. This phenomenon indicated that such a silica matrix has nanocage structure with many holes on the surface of the shell part. Based on the data from Gaussian 03 calculations and the CRC handbook, the molecular diameter of TA and I^- is about 0.624 and 0.440 nm, respectively. So, the diameter of the holes on the surface of silica nanoparticles was smaller than 0.624 nm but bigger than 0.440 nm (Fig. 2C). Such a scale can ensure that HA–GQD (bigger than 1 nm) was big enough and cannot leak from the nanoparticle matrix but O_2 and $^1O_2$ (0.360 nm in diameter) were small enough and can easily pass in and out of the nanoparticles from the holes to make sure the PDT efficacy.

Many reports indicate that after being encapsulated inside silica nanoparticles, the fluorescence intensity of fluorescent materials would greatly increase, which is helpful for their *in vitro* fluorescence imaging.[2d,10,13] The 3D-fluorescence contour map of HA–GQD and HA–GQD–SiO_2 was studied because it could provide detailed fluorescence information (Fig. 3). Two typical fluorescence peaks, peak 1 (GQD portion) and peak 2 (HA portion), could be observed in the 3D-fluorescence contour map of HA–GQD and HA–GQD–SiO_2. After being encapsulated inside silica nanoparticles, the fluorescence peak shifted and the intensities of peaks 1 and 2 were all greatly improved (Table S3, ESI†).

The absence of fluorescence of the nonpolar compound dispersed in a polar solvent can be due to either drug–solvent interaction promoting nonradiative decay or concentration quenching derived from self-aggregation of nonpolar compounds.[2d] Furthermore, many reports indicated that the more uniform size distribution of carbon related quantum dots results in higher fluorescence intensity.[13,14] Similar to previous reports, the fluorescence emission intensity of HA–GQD–SiO_2 was much stronger than HA–GQD possibly due to size confinement together, in part, with elimination of aggregates for HA–GQD. Besides, silica shell protected HA–GQD from exposure to an aqueous environment that could cause a partial loss of fluorescence. The property of resistance to fluorescence quenching in aqueous media by entrapped HA–GQD inside silica nanoparticles can be exploited to fabricate nanoprobes for imaging in biological systems. Furthermore, the lifetime, fluorescence quantum yield, and fluorescence stability of the GQD portion and the HA portion for HA–GQD were all improved (Fig. S6 and S7, Tables S4 and S5, ESI†) after being encapsulated inside silica nanoparticles, and such an increased lifetime would be helpful for the $^1O_2$ generation by HA–GQD–SiO_2.

$^1O_2$, the main cytotoxic agent involved in the eradication of cancer cells,[15] was detected using the sodium salt of 9,10-anthracenedipropionic acid (ADPA) as a sensor by a classic method.[2d] Fig. 4A shows the decay curve for HA–GQD–SiO_2 in aqueous solution with ADPA (the decay curves of HA, HA–GQD, GQD and SiO_2 are shown in Fig. S8, ESI†), which shows a sharp decrease in absorbance intensity with the light exposure time, indicating the generation of $^1O_2$ by HA–GQD–SiO_2. According to the classic equations reported by Raoul Kopelman's group, the exact reaction rate constant (k) with ADPA for HA (1.23×10^{-3}), HA–GQD (1.41×10^{-3}), HA–GQD–SiO_2 (2.09×10^{-3}), GQD (0.11×10^{-3}) and SiO_2 (0.08×10^{-3}) in our experiment was calculated from Fig. 4B, respectively. Compared with HA–GQD, the k value of HA–GQD–SiO_2 was obviously increased, which indicated the improved $^1O_2$ generation ability of HA–GQD after being encapsulated inside silica nanoparticles. There are two reasons for the increased $^1O_2$ generation ability of HA–GQD–SiO_2. The first one was the prevention of quenching of energy transfer steps before $^1O_2$ generation (due to aggregation). The second one was the protection effect of encapsulation, which partly prevents the quenching of $^1O_2$.[2d,16] Such increased $^1O_2$ generation ability implied that HA–GQD–SiO_2 may have superior PDT efficacy to HA–GQD in the PDT process.

Fluorescence imaging was used to determine whether HA–GQD–SiO_2 was taken up by tumor cells and its fluorescence signal properties. Cervical cancer is both the fourth most common cause of cancer and the fourth most common cause of death from cancer in women worldwide. Research studies indicated that cervical cancer could be treated through PDT with the help of optical fiber, endoscope and many interventional techniques to lead the laser directly to the lesion location inside the body. So, here, human

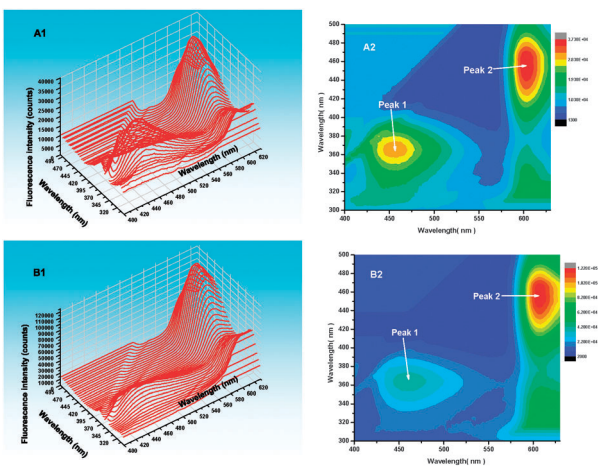

Fig. 3 Three-dimensional surface projections (1) and the false color map with contour spectra (2) of HA–GQD (A) and HA–GQD–SiO_2 (B).

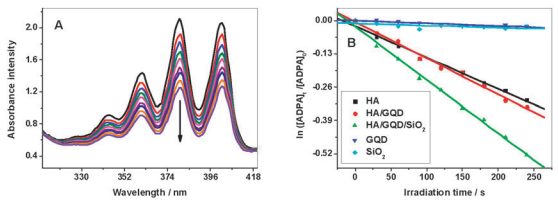

Fig. 4 Absorption spectra of HA–GQD–SiO_2 with ADPA (A) irradiated for 0, 30, 60, 90, 120, 150, 180, 210 and 240 s by light and the reaction rate constant comparison (B).

Published on 11 November 2014. Downloaded by Michigan State University on 20/01/2016 17:53:46.

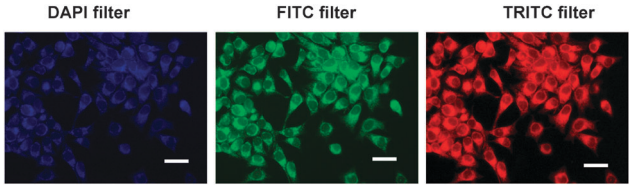

Fig. 5 The fluorescence microscopy images of HeLa cells treated with HA–GQD–SiO_2 at various excitation wavelengths by different filters (instrument details in ESI†).

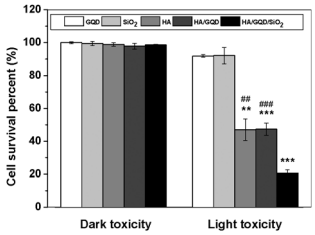

Fig. 6 Comparative *in vitro* dark toxicity and light toxicity of HA, HA–GQD, HA–GQD–SiO_2, GQD and SiO_2 (**$p < 0.01$ dark toxicity *vs.* light toxicity of same drug; ***$p < 0.001$ dark toxicity *vs.* light toxicity of same drug; $^{\#\#}p < 0.01$ light toxicity of HA *vs.* light toxicity of HA–GQD–SiO_2; $^{\#\#\#}p < 0.001$ light toxicity of HA–GQD *vs.* light toxicity of HA–GQD–SiO_2).

cervical carcinoma cells (HeLa) were used for our *in vitro* imaging and anticancer studies. The cellular uptake of HA–GQD–SiO_2 and intracellular fluorescence images are shown in Fig. 5. The fluorescence images of HeLa cells, treated with HA–GQD–SiO_2, show significant intracellular staining in the cytoplasm, indicating the accumulation of HA–GQD–SiO_2. Besides, strong blue, green and red fluorescence was detected inside the cancer cells with similar distribution patterns obtained for fluorescence from HA–GQD–SiO_2 with low photobleaching. These results indicated that HA–GQD–SiO_2 is an effective probe for bioimaging.

To get a more quantitative PDT induced anticancer activity of the above drugs, the inhibitory rates to HeLa cells were detected by cell morphology analysis and MTT assay. Fig. 6 shows the cell survival percentages after being treated with various drugs, including HA, HA–GQD, HA–GQD–SiO_2, GQD and SiO_2, under dark conditions using the untreated cells as control. Results indicated that all of the drugs have low dark toxicity to HeLa cells. On the contrary, the obvious morphology change and cell death can be observed for HA, HA–GQD and HA–GQD–SiO_2 after irradiation (Fig. S9, ESI†). Almost no cellular light-induced toxicity can be observed for GQDs and SiO_2. In addition, HA–GQD–SiO_2 exhibited an enhanced phototoxic effect over HA and HA–GQD possibly because of its superior $^1O_2$ generation ability to HA and HA–GQD. The above results show the potential of HA–GQD–SiO_2 for improving the actual efficacy of PDT.

In summary, to obtain a theranostic drug, combining both multicolor imaging and treatment, in the field of diagnostics and PDT for superficial cancer, the complex of HA, a photosensitive anti-cancer drug, and fluorescent GQDs was prepared through π–π stacking interaction. The interaction mechanism between HA and GQDs through energy and electron transfer was systematically studied. For the purpose of avoiding the complex being destroyed during the drug delivery process, the complex was encapsulated inside porous silica nanoparticles. Research studies indicated that the fluorescence signal intensity and the *in vitro* PDT effect towards cancer cells of HA–GQD were significantly increased after being encapsulated inside the particles, which demonstrated the validity and potential of HA–GQD–SiO_2 as a theranostic regent in the field of PDT.

We are grateful for financial support from the National Natural Science Foundation of China (21201102), The Natural Science Foundation of Jiangsu Higher Education Institutions of China (No. 13KJA150003 and 12KJB150015), The Priority Academic Program Development of Jiangsu Higher Education Institutions (PAPD) and Jiangsu Collaborative Innovation Centre of Biomedical Functional Materials.

Notes and references

1 S. D. Topel, G. T. Cin and E. U. Akkaya, *Chem. Commun.*, 2014, **50**, 8896.
2 (*a*) S. B. Brown, E. A. Brown and I. Walker, *Lancet Oncol.*, 2004, **5**, 497; (*b*) D. Dolmans, D. Fukumura and R. K. Jain, *Nat. Rev. Cancer*, 2003, **3**, 380; (*c*) S. Kim, T. Y. Ohulchanskyy, H. E. Pudavar, R. K. Pandey and P. N. Prasad, *J. Am. Chem. Soc.*, 2007, **129**, 2669; (*d*) I. Roy, T. Y. Ohulchanskyy, H. E. Pudavar, E. J. Bergey, A. R. Oseroff, J. Morgan, T. J. Dougherty and P. N. Prasad, *J. Am. Chem. Soc.*, 2003, **125**, 7860.
3 (*a*) P. Huang, J. Lin, X. S. Wang, Z. Wang, C. L. Zhang, M. He, K. Wang, F. Chen, Z. M. Li, G. X. Shen, D. X. Cui and X. Y. Chen, *Adv. Mater.*, 2012, **24**, 5104; (*b*) L. B. Josefsen and R. W. Boyle, *Theranostics*, 2012, **2**, 916; (*c*) S. S. Kelkar and T. M. Reineke, *Bioconjugate Chem.*, 2011, **22**, 1879; (*d*) T. Krasia-Christoforou and T. K. Georgiou, *J. Mater. Chem. B*, 2013, **1**, 3002.
4 Q. B. Xiao, Y. T. Ji, Z. H. Xiao, Y. Zhang, H. Z. Lin and Q. B. Wang, *Chem. Commun.*, 2013, **49**, 1527.
5 Z. J. Gu, L. Yan, G. Tian, S. J. Li, Z. F. Chai and Y. L. Zhao, *Adv. Mater.*, 2013, **25**, 3758.
6 (*a*) J. Xie, J. H. Ma and J. Q. Zhao, *Sci. China, Ser. B: Chem.*, 2002, **45**, 251; (*b*) H. Kobayashi, M. Ogawa, R. Alford, P. L. Choyke and Y. Urano, *Chem. Rev.*, 2010, **110**, 2620.
7 J. H. Zhou, S. Q. Xia, J. R. Chen, X. S. Wang and B. W. Zhang, *Chem. Commun.*, 2003, 1372.
8 Y. Zhang, L. M. Song, J. Xie, H. X. Qiu, Y. Gu and J. Q. Zhao, *Photochem. Photobiol.*, 2010, **86**, 667.
9 (*a*) Z. S. Qian, J. J. Ma, X. Y. Shan, L. X. Shao, J. Zhou, J. R. Chen and H. Feng, *RSC Adv.*, 2013, **3**, 14571; (*b*) X. Guo, C. F. Wang, Z. Y. Yu, L. Chen and S. Chen, *Chem. Commun.*, 2012, **48**, 2692; (*c*) B. Z. Ristic, M. M. Milenkovic, I. R. Dakic, B. M. Todorovic-Markovic, M. S. Milosavljevic, M. D. Budimir, V. G. Paunovic, M. D. Dramicanin, Z. M. Markovic and V. S. Trajkovic, *Biomaterials*, 2014, **35**, 4428; (*d*) S. N. Baker and G. A. Baker, *Angew. Chem., Int. Ed.*, 2010, **49**, 6726; (*e*) J. H. Shen, Y. H. Zhu, X. L. Yang and C. Z. Li, *Chem. Commun.*, 2012, **48**, 3686.
10 L. Zhou, J. H. Liu, J. Zhang, S. H. Wei, Y. Y. Feng, J. H. Zhou, B. Y. Yu and J. Shen, *Int. J. Pharm.*, 2010, **386**, 131.
11 H. F. Dong, W. C. Gao, F. Yan, H. X. Ji and H. X. Ju, *Anal. Chem.*, 2010, **82**, 5511.
12 P. Yu, X. M. Wen, Y. R. Toh, Y. C. Lee, K. Y. Huang, S. J. Huang, S. Shrestha, G. Conibeer and J. Tang, *J. Mater. Chem. C*, 2014, **2**, 2894.
13 C. W. Lai, Y. H. Hsiao, Y. K. Peng and P. T. Chou, *J. Mater. Chem.*, 2012, **22**, 14403.
14 X. Wang, L. Cao, S. T. Yang, F. S. Lu, M. J. Meziani, L. L. Tian, K. W. Sun, M. A. Bloodgood and Y. P. Sun, *Angew. Chem., Int. Ed.*, 2010, **49**, 5310.
15 A. Sivery, A. Barras, R. Boukherroub, C. Pierlot, J. M. Aubry, F. Anquez and E. Courtade, *J. Phys. Chem. C*, 2014, **118**, 2885.
16 L. Zhou, S. H. Wei, X. F. Ge, J. H. Zhou, B. Y. Yu and J. Shen, *J. Phys. Chem. B*, 2012, **116**, 12744.

 This journal is © The Royal Society of Chemistry 2015